Research on Engineering Structures & Materials
www.jresm.org
MIM Research Group

Research Article

Influence of samarium oxide mixing on the structural and optical properties of tin oxide thin films prepared by pulsed laser deposition

Noor Sadie Saleh [a], Jamal M. Rzaij [*,b]

Department of Physics, College of Science, University Of Anbar, Ramadi, Iraq

Article Info

Article History:

Received 06 Dec 2024

Accepted 15 Apr 2025

Keywords:

Sn;
Structural and optical properties;
Rare–earth elements;
Optoelectronic applications

Abstract

Due to the growing demand for optoelectronic applications, it is imperative to investigate the properties of thin films and identify the most suitable ones for use in optical detectors, gas sensors, and solar cells. In a novel investigation, this work analyses the impact of samarium oxide (Sm_2O_3) mixing at varying weight ratios (5, 7, and 9 wt.%) on the structural, morphological, and optical properties of tin oxide (Sn) films deposited by pulsed laser deposition (PLD). XRD analysis confirmed the crystallization of a polycrystalline structure of SnO_2 and SnO phases (SnOx). The crystallite size decreased from 13.1 nm to 7.2 nm with samarium content up to 7 wt.% and then increased to 11.3 nm at 9 wt.%. Top-view field emission scanning electron microscopy (FE-SEM) images revealed a broad particle size distribution that fluctuated with the Sm_2O_3 mixing ratio, exhibiting an average diameter of 44.53–35 nm. The incorporation of Sm_2O_3 elevated the film thickness to 629 nm at the maximum ratio. Atomic emissions of Sn, Sm, and O elements were identified using Energy-dispersive X-ray spectroscopy (EDX), and elemental mapping verified the homogeneous distribution of Sm into the SnOx film's surface. UV-visible transmittance spectra showed decreased transmittance from 80% to 63% at a higher Sm_2O_3 mixing ratio. In contrast, photoluminescence (PL) spectra exhibited a red emission peak shift, which reduced the optical bandgap from 3.4 eV to 3.15 eV. The results indicate that Sm_2O_3-mixed SnOx thin films exhibit adjustable characteristics appropriate for optoelectronic and catalytic applications.

1. Introduction

Transparent conducting oxides (TCO) are outstanding semiconductors with high electrical conductivity and a wide transmittance in the visible spectrum. The applications of TCO materials are widely used in research and technology due to their distinctive qualities. Deep studies on the wide optical band gap of semiconducting metal oxides, such as Ti, ZnO, GaN, In2O3, and Sn, have been conducted over the past few decades and are still highly active materials being studied recently. Because of its greater stability in ambient circumstances, stability at high temperatures, mechanical hardness, and chemically inert properties. Sn is one of the most widely used materials among the available TCOs [1,2].

Among transparent conducting oxides, tin dioxide is an n-type semiconductor with a negative majority of charge carriers (n-type) and a tetragonal crystal structure. Due to its broadband gap (about 3.6 eV), it is a promising option for optoelectronic applications such as gas sensors, light-emitting diodes (LEDs), phototransistors, and solar cell window layers [3].

*Corresponding author: sc.jam72al@uoanbar.edu.iq
[a]orcid.org/0009-0003-1954-514X; [b]orcid.org/0000-0003-2287-3083
DOI: http://dx.doi.org/10.17515/resm2025-566ma1206rs

Pure Sn thin films have limited use in many optoelectronic device applications because of their low carrier density and mobility. The electrical conductivity and optical transmittance of Sn are typically caused by oxygen vacancies in the crystal lattice [4]. Several suggestions have been investigated for doping tin oxide with metal ions, such as Sm [5], Eu [6], and Gd [1], or semiconductor oxides, such as Sn:CdO [7], CdS: Sn [8], and ZnO: Sn [9], to enhance its physical and chemical characteristics for employment in the applications mentioned earlier. Previous researchers have employed various deposition techniques, including magnetron sputtering [10], Sol-gel [11], hydrothermal route [12], and spray pyrolysis [2], to develop thin tin oxide coatings in nanosized structures. Thin films of Sn were prepared by Emeka Charles et al. [13] using metalorganic precursors on glass substrates at different annealing temperatures. The synthetic results showed that the films deposited at an annealing temperature of 500 °C were polycrystalline with a tetragonal structure, while those deposited at 250 °C were random. The surface morphology results confirmed the presence of nanometer-sized particles, which increased with rising annealing temperature. The absorption spectra showed that the energy gap decreased with increasing annealing temperature, while the deposited films' transmittance reached its peak (83.2%) at a wavelength around 350 nm. The conclusions confirmed that the Ti films show promising properties at annealing temperatures around 500 °C.

Thin films of Sn doped with Sm_2O_3 at different weight percentages were deposited by Ahmadnia-Feyzabad et al. using a chloride solution combustion calcined at 400 °C in the air for gas sensor applications [14]. The diffraction index of the polycrystalline samples is indexed to the tetragonal rutile structure of Sn, and no peak corresponds to Sm_2O_3. When the wt.% of Sm_2O_3 reached its maximum, the size of the particles increased from less than 100 nm to more than 300 nm. Sm_2O_3 alters the reaction mechanism, reduces the crystallite sizes of nanoparticles, raises the concentration of oxygen vacancies, and modifies the catalytic activity of the Sn sensing characteristics. Singkammo et al. [15] used flame spray pyrolysis to create Sn thin films doped with 0.1-2 wt% Sm_2O_3 nanoparticles. The study concentrated on Sm_2O_3's catalytic properties and their effects on C2H4O sensing features. XRD investigation revealed a highly sharp peak of the tetragonal Sn structure with an average crystallite size of 10 nm. The top-view SEM images of Sm-doped Sn nanoparticles show agglomerated nanoparticles with particle sizes of less than 50 nm. The gas sensing results indicated that the incorporation of Sm_2O_3 enhanced the sensitivity of the Sn thin film by approximately sixfold relative to the as-deposited sample.

Researchers in most of the above studies reported the Sn deposition using chemical deposition methods. One drawback of chemical deposition methods is that they involve high deposition temperatures. In contrast, physical methods can develop thin films of high homogeneity and purity at comparatively low temperatures. Moreover, compared to physical techniques, chemical procedures are more expensive and complicated and can be connected with hazards. An important physical method for depositing different metals, oxides, sulfates, and nitrides is pulsed laser deposition (PLD) [16]. The basic principle of PLD is the interaction of a high-energy laser beam with the target material inside a vacuum chamber to develop a plasma plume driving the ablated material toward the deposition substrate. The technique yields high-purity thin films while preserving the stoichiometry material, enabling precise control over the thickness of the formed films at a relatively rapid deposition rate. However, PLD can suffer from particulate contamination and limited area uniformity, and expensive laser systems and vacuum chambers are required. The discrete nature of target material delivery in PLD results in a plasma plume with energetic species, such as ions, atoms, and molecules, that deposit on the substrate [17–20].

The rare-earth elements are interesting dopants due to their unique electronic and optical properties. Rare-earth doping/mixing can improve semiconductor oxides' structural, optical, and electrical characteristics by introducing additional charge carriers, which is beneficial for numerous applications. They can also enhance reactivity by creating more active sites on their surface for gas sensing or catalysis applications [21]. Additionally, rare-earth elements can modify the optical properties of Sn by introducing new energy levels within its band gap, enhancing optoelectronic and sensing features [22,23]. The incorporation of rare-earth elements, such as samarium atoms, into catalyst materials results in a reduction in crystal size, an increase in surface area, and exceptional stability in chemical reactions [24]. Furthermore, the occupied Sm, a

substitutional site of Sn in the crystal lattice of Sn, demonstrates donor-like characteristics, whereas oxygen vacancies function as acceptors [25]. This study investigated the impact of mixing samarium oxide at varying weight ratios on the structural, morphological, and optical characteristics of tin oxide films deposited via the pulsed laser deposition technique.

2. Experimental

2.1 Substrate Cleaning

The prepared films were deposited on soda lime glass substrates measuring 2.5×2.5 cm to investigate their optical properties after they were washed with distilled water and detergent solution. They were subsequently cleaned ultrasonically in ethanol for fifteen minutes and finally dried with a dryer. Moreover, silicon wafers measuring 1.5×1.5 cm were used to examine the deposited films' structural characteristics and surface morphology. The silicon wafers were cleansed using a Hydrofluoric acid (HF) solution diluted with water at a 1:5 ratio, subsequently rinsed with distilled water to eliminate residual acid, then immersed in an ethanol bath for fifteen minutes and dried with a dryer.

2.2 Materials and Methods

A Q-switching pulsed ND-YAG laser system (Smart Pico, Deka, Italy) with double wavelengths of 1064 nm and 532 nm was used to deposit unmixed and Sm_2O_3 mixed-Sn thin films at varying weight percentages (5, 7, and 9 wt.%) on n-type silicon substrates. The deposition chamber comprises a holder supporting a rotating base (35 rpm), upon which the target is affixed to avoid fast etching and uniform ablation of the target. The substrate holder is positioned approximately 4 cm vertically above the substrate holder. A tin oxide target, measuring 0.5 cm in thickness and 3 cm in diameter, was formed using 5 gm of Sn powder utilizing a hydraulic press at about 118 kPa for 24 hours to enhance atomic cohesion within the compressed target disc. This increased its stability and density, improving the deposited film's quality. The resulting target was condensed by annealing at 550 °C for 2 hours in air. The SnO_2 target was selectively ablated at room temperature (~28 °C) using an Nd-YAG laser with a wavelength of 1064 nm, pulse energy of 700 mJ, pulse frequency of 6 Hz, pulse duration of 9 nanoseconds, a focal spot area of 12.56 mm^2, an energy density of 55.73 mJ/mm^2 per laser pulse, and a total of 700 pulses. Fig. 1 illustrates the schematic diagram of the pulsed laser deposition system.

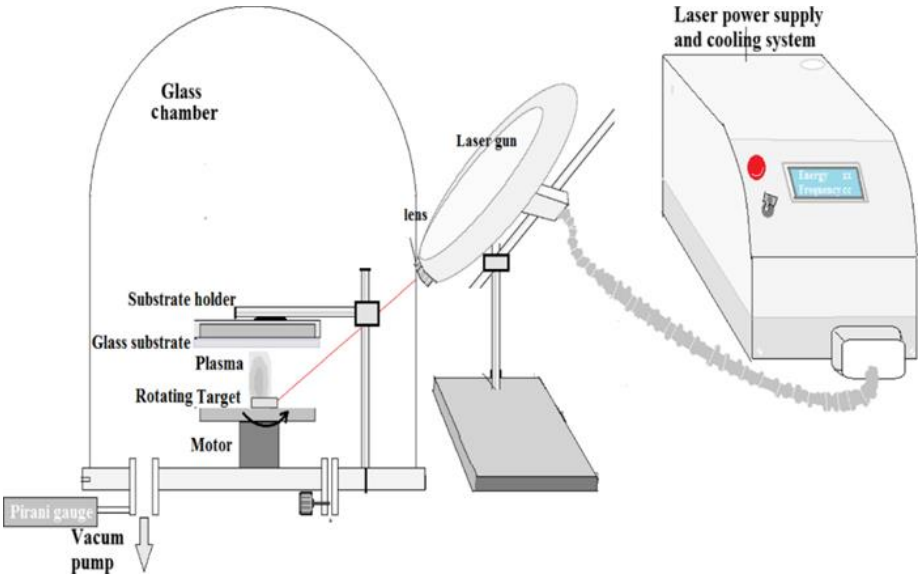

Fig. 1. Schematic diagram of pulsed laser deposition system

The impulse and coupling coefficient at varying pressures depend on the target's ablation and plasma characteristics, which are affected by the laser wavelength. As the wavelength of the laser decreases, there is a corresponding increase in both the depth of the crater and the bulk of the ablated material. Under atmospheric pressure, the plasma plume tends to disperse, whereas its

length continuously extends in low-pressure conditions. This leads to a plasma comprising more ablated particles exhibiting increased velocities, enhancing both the impulse and coupling coefficients [26]. Thus, in this work, the deposition chamber was evacuated to 20 Pa, and a laser pulse with a wavelength of 1064 nm was used to achieve more uniform thin film coatings and decrease the mean free path of the ablated particles. Finally, the deposited films were annealed at 500°C in air for 2 hours. To obtain SnO_2 targets mixed with Sm_2O_3, the previous procedure was repeated with 5, 7, and 9 wt.% Sm_2O_3 mixed. SnO_2 and Sm_2O_3 powders were purchased from Aldrich Chem., USA, with a high purity of 99.98%.

2.3 Thin Film Characterization

A Dandong Haoyuan DX-2700B XRD with a Cu-Kα source was employed at ambient temperature to examine crystalline structures. A diffraction angle (2θ) range of 10° to 80° with an X-ray wavelength of 1.54056 Å. The surface morphology of SnO_2 thin films was examined using a Field Emission Scanning Electron Microscope (FE-SEM, MIRA3 diffractometer (TESCAN)) equipped with energy-dispersive X-ray Spectroscopy. The optical properties of the developed thin films were investigated by depositing them on glass substrates and detecting the optical absorption spectra. Spectral measurements were conducted with a dual-beam UV-Vis spectrometer manufactured in England, with a 200 to 900 nm spectral range. The Photoluminescence (PL) analysis was performed utilizing the FluoroMate FS-2 spectrometer manufactured by Scinco, Korea. The excitation wavelength was 290 nm at room temperature, and the detection range ranged from 300 to 600 nm.

3. Results and Discussions

3.1 X-ray Diffraction

Fig. 2 shows the as-deposited and SnO_x XRD patterns mixed with Sm_2O_3 at different concentrations (5, 7, and 9 wt.%) of thin films by pulsed laser deposition technique. Polycrystalline structure of mixed phases of the dominant orthorhombic SnO with tetragonal SnO_2 structure according to standard PDF cards 000-55-0837 and 010–75-9495, respectively. The matching result was obtained by Nikiforov et al. using the molecular beam epitaxy deposition method [27].

The XRD pattern verified the crystallization of the polycrystalline structure of SnO_2 and SnO phases, which agrees with the previous studies [28,29]. Given that the fabricated films were produced using laser ablation in a vacuum environment, a significant concentration of oxygen vacancies will be expected. When atoms of the target material are ablated in a vacuum to be deposited on the substrate at room temperature, the diffusion length of similar atoms on the substrate's surface is small, inhibiting the movement of the ablated atoms. The restricted mobility of similar atoms supports the formation of polycrystalline structure films instead of a single crystalline structure [30]. Moreover, the enrichment of Sn on the target surface due to interaction with the plasma plume considerably elevates the Sn concentration in the films, enhancing its stoichiometric content in the SnO_2 structure [31]. The substitution of Sn by Sm causes nearest-neighboured oxygen vacancies, causing an increase in the crystallinity of the as-deposited SnO_2 compared with the SnO_2 mixed samples [32].

A crucial crystallographic characteristic is the crystallite size (D), determined using Scherrer's formula (Eq (1)) [33], which corresponds to the dominant diffraction peaks of the SnO and SnO_2 phases.

$$D = k\lambda/\beta\ cos\theta \tag{1}$$

where λ represents the X-ray wavelength, θ denotes the diffraction angle in radians, and k signifies the Scherrer correction factor (k=0.89).

Table 1 lists the diffraction angles (2θ), Full width at half maximum (β), interplanar distance (d_{hkl}), crystallite size (D), and the stress ($\boldsymbol{\varepsilon}$) of the deposited films. It illustrates a reduction in crystallite size from 13.1 nm to 7.2 nm with the increment of samarium content up to 7 at wt.%, followed by an increase to 11.3 nm when the samarium oxide content attains 9 wt.%. However, the effect of

samarium oxide mixing effectively decreased the deposited films' crystal size. The reduction in crystal size can be attributed to the incorporation of samarium oxide in the tin oxide lattice. The crystal deformation caused by the incorporation of samarium in the tin oxide lattice can be determined by calculating the stress (Eq (2)) [34], which corresponds to the stress related to the diffraction peak width.

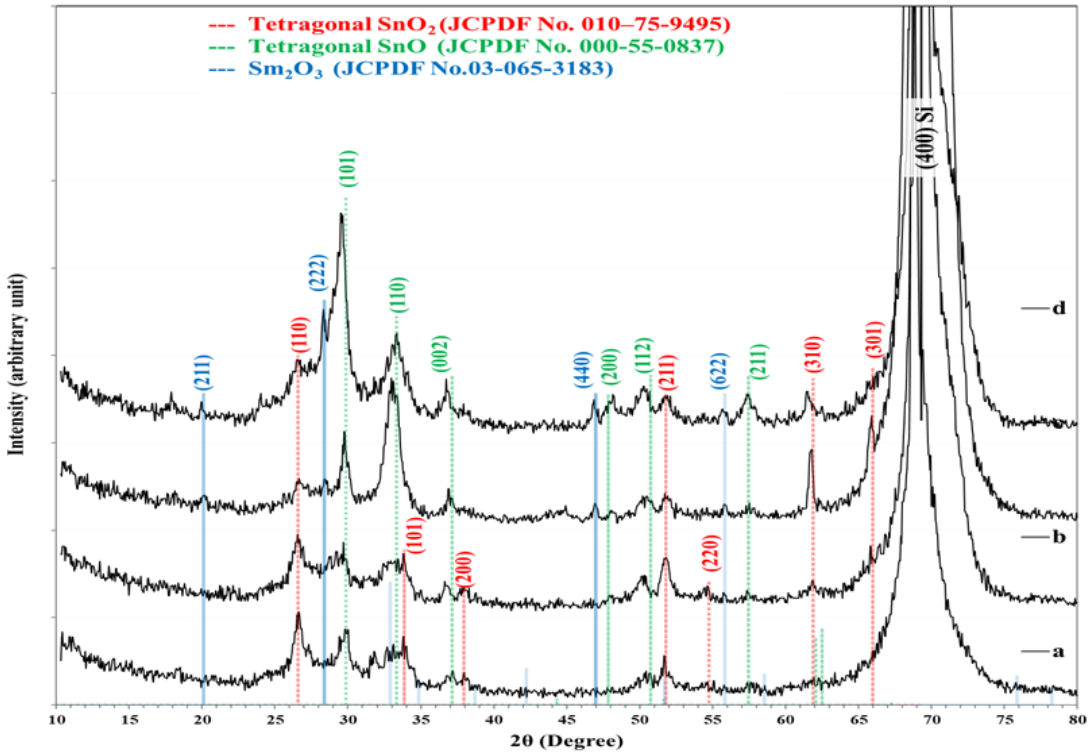

Fig. 2. XRD patterns of (a) the as-deposited SnO_2, (b) 5 wt.% Sm_2O_3 mixed-SnO_x, (c) 7 wt.% Sm_2O_3 mixed-SnO_x, and (d) 9% Sm_2O_3 mixed-SnO_x

$$\varepsilon\ (\%) = \beta/4\ tan\theta \tag{2}$$

The stress induced by samarium within the tin oxide lattice inhibits the development of tin oxide crystals and limits the movement of grain boundaries, as illustrated in Table 1. Singkammo *et al.* [15] reported a comparable outcome. In optoelectronic applications, reduced nano-sized crystal dimensions provide an increased surface area for the interaction with target gas molecules and/or incident light, enhancing the interaction with gas and/or optical detectors and markedly improving their responsiveness [35].

Table 1. Diffraction angle and crystallite size corresponding to the dominant diffraction peak at various Sm_2O_3 concentrations

Sm_2O_3%	2θ (Deg.)	β (Deg.)	β (rad)	d_{hkl} (Å)	D (nm)	(hkl)	Phase	ε(%)
0	26.5835	0.651	0.0114	3.3504	13.1	(110)	SnO_2	1.20
5	26.5492	0.7881	0.0138	3.3547	10.8	(110)	SnO_2	1.46
7	32.9907	1.1992	0.0209	2.7129	7.2	(110)	SnO	1.77
9	29.5672	0.758	0.0132	3.0188	11.3	(101)	SnO	1.25

The examination of the structural characteristics of the deposited films confirmed that an increase in Sm_2O_3 wt.% resulted in a slight shift of the diffraction peaks towards lower diffraction angles, signifying an increase in the crystal lattice constants, as illustrated in Table 2. The lattice constants of the prepared films were calculated based on the dominant diffraction peak of each diffraction

pattern. The increased value of the lattice constants is ascribed to the larger atomic radius of samarium (185 pm) relative to that of tin (145 pm). An identical investigation has been reported by Shaikh *et al*. [36].

Table 2. Lattice parameters of SnO_2 and SnO at various Sm_2O_3 wt.% contents.

Sm_2O_3 wt.%	SnO_2		SnO	
	a (Å)	c (Å)	a (Å)	c (Å)
0	4.72281	3.18377	3.80041	4.83804
5	4.72629	3.18432	3.80648	4.86839
7	4.72826	3.18551	3.81613	4.87713
9	4.73326	3.18639	3.81677	4.89031

3.2 Surface Morphology Analysis

Fig. 3a presents the top view of FE-SEM images at two magnifications, along with a histogram illustrating the particle size distribution of SnO_x as it is deposited and mixed with Sm_2O_3 thin films. The SnO_x thin films have a broad surface interlaced with randomly distributed spherical nanoparticles. The histogram depicts a diverse particle size distribution ranging from 10 nm to 200 nm, with a mean diameter of 44.53 nm and a standard deviation of 27.1 nm; the analysis was determined by ImageJ software. The incorporation of Sm_2O_3 into SnO_x at varying wt.% considerably impacts particle diameter and distribution, hence changing the characteristics of the samples. As shown in Fig. 3b, the average particle diameter decreased to 25.74 nm at a 5 wt.% Sm_2O_3 mixing ratio, with a standard deviation of 11.0 nm. The Sm_2O_3 addition reduced the size distribution to between 10 and 45 nm, in contrast to the as-deposited SnO_x sample, indicating a homogeneous particle size distribution. At a 7 wt.% Sm_2O_3 mixing ratio (Fig. 3c), the average particle diameter increased to 26.4 nm, with a standard deviation of 15 nm. However, the average particle diameter increased to 35.2 nm, with a standard deviation of 17.8 nm, indicating a broader size distribution when the Sm_2O_3 mixing ratio reached 9 wt.% (Fig. 3d).

The incorporation of Sm_2O_3 reduced the particle diameter, resulting in deposited surfaces with an enhanced surface area-to-volume ratio; smaller particles augment this ratio, thus improving the film's reactivity, adsorption capacity, or catalytic efficiency. These alterations are substantial in applications such as coatings, sensors, or electronic devices, where particle size directly influences performance [37,38]. Adding samarium oxide also controls grain development, resulting in a reduced, more homogenous structure that improves mechanical characteristics. The narrow, homogenous distribution raises the threshold electric field to enhance variable varistors' non-linear electrical characteristics. Moreover, the films' high surface-to-volume ratio enhances oxidation and reduction reactions when used as gas sensors [35,39].

Cross-sectional scanning electron microscope images (Fig. 4a-d) indicated that the thickness of the SnO/SnO_2 thin films increased from 376 nm to 629 nm with increasing Sm_2O_3 content; the analysis was determined by ImageJ software. Film thickness increase can be explained by including Sm in the SnO_x lattice, which is attributed to the ionic/atomic diameter disparity between tin and samarium. This discrepancy increased interatomic distance inside the crystal lattice, enhancing lattice parameters, confirmed by structural analysis results, and, ultimately, a thicker deposited layer [40–42]. This is demonstrated in Fig. (4-d), which indicates that the film incorporating 9 wt.% samarium oxide, the maximum mixing ratio, exhibited the highest thickness.

Fig. 5 shows the variation in the thickness as a function of the Sm_2O_3 wt.% thin films with the standard deviation value. Adding Sm_2O_3 to SnO/SnO_2 films can be crucial in controlling their thickness. This control over thickness is essential for various applications, such as gas sensors, catalysis, and optoelectronic devices, where specific film thicknesses are required for optimal performance.

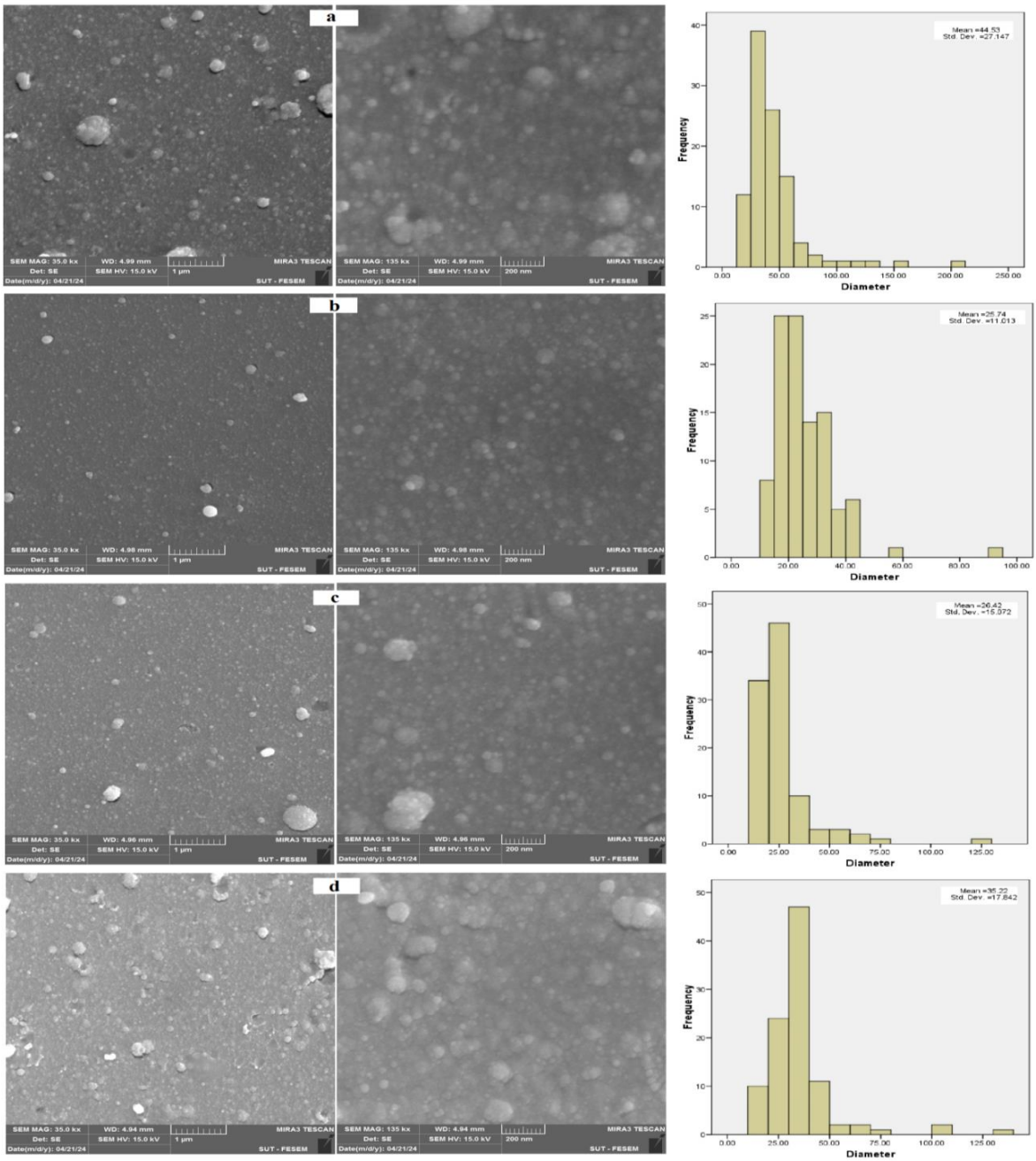

Fig. 3. Top-view FE-SEM images and particle diameter distribution (a) the as-deposited SnO_x, (b) 5 wt.% Sm_2O_3 mixed-SnO_x, (c) 7 wt.% Sm_2O_3 mixed-SnO_x, and (d) 9% Sm_2O_3 mixed-SnO_x

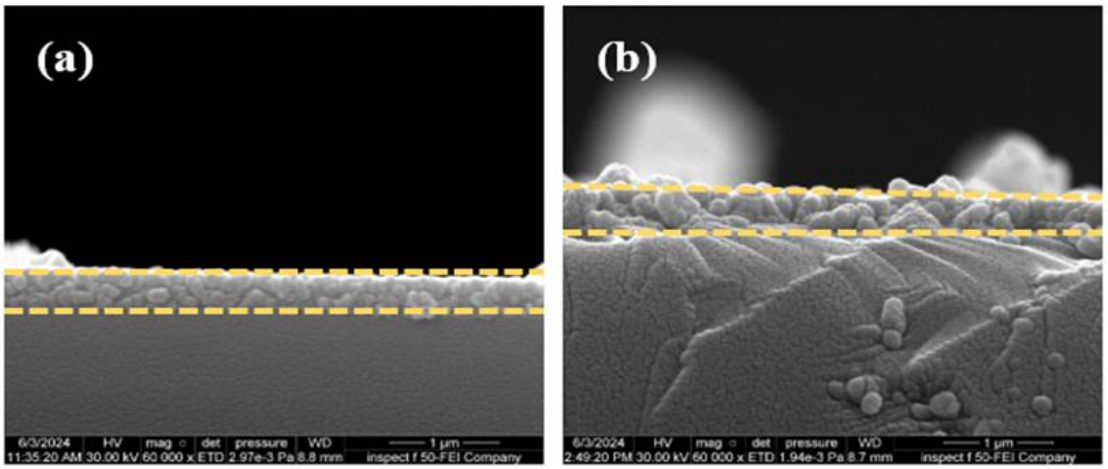

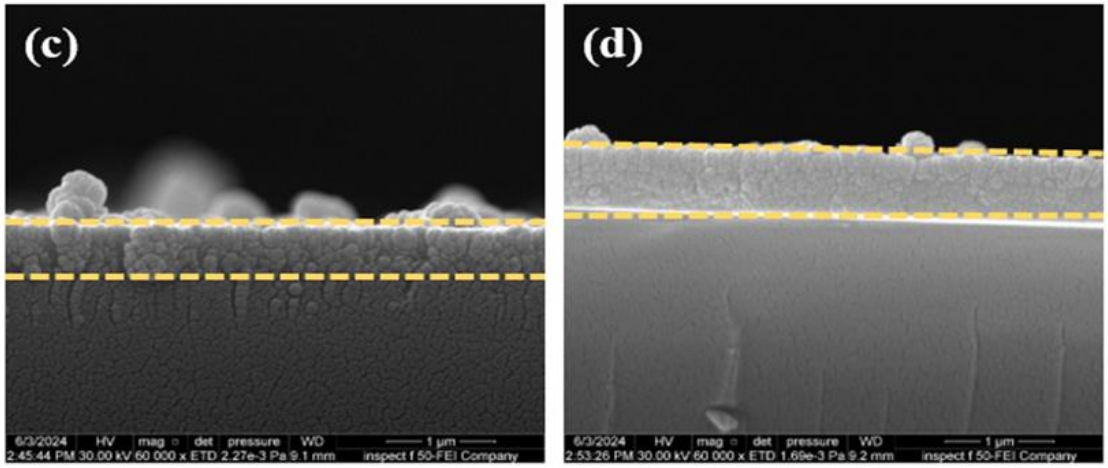

Fig. 4. Cross-sectional FE-SEM images of (a) the as-deposited SnO_x, (b) 5 wt.% Sm_2O_3 mixed-SnO_x, (c) 7 wt.% Sm_2O_3 mixed-SnO_x, and (d) 9% Sm_2O_3 mixed-SnO_x

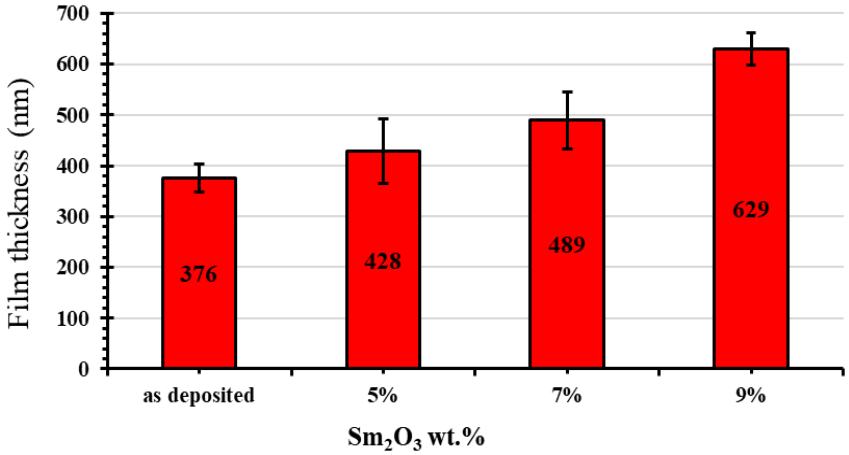

Fig. 5. Thickness variation of SnO_x as a function of the Sm_2O_3 wt.% thin films (The bar represents the standard deviation)

3.3 EDS Spectra Analysis

EDS spectra of the as-deposited SnO/SnO_2 and Sm_2O_3-mixed SnO/SnO_2 thin films at various mixing ratios are illustrated in Fig. 6(a-d). Atomic emissions of Sn, Sm, and O elements were detected. A significant peak at 1.7 keV, corresponding to Si emission from the Si substrate, was also observed. Additionally, an Au emission peak was present due to the prior deposition of a gold layer onto the samples as a preparatory step for SEM testing.

Table 3. Elemental analysis of Sm_2O_3 mixed-SnO_x at various mixing ratios

Sample	Element	Wt%	Atomic %
SnOx	O	28.27	74.21
	Sn	71.73	25.79
5% Sm_2O_3	O	29.69	75.9
	Sn	68.61	23.64
	Sm	1.7	0.46
7% Sm_2O_3	O	21.99	67.8
	Sn	75.55	31.4
	Sm	2.45	0.81
9% Sm_2O_3	O	22.89	69.02
	Sn	72.95	29.65
	Sm	4.15	1.33

These two peaks were neglected when determining element ratios. The decreased intensity of the O emission peak with increasing Sm_2O_3 content indicates a reduced incorporation of O atoms within the lattice, as listed in Table 3. Furthermore, the incorporation of Sm_2O_3 resulted in the development of Sm emission peaks, which correlated with a rise in the weight percentage of the film's components associated with Sm_2O_3 content. The EDS map shown next to the spectra, corresponding to Sn, O, and Sm atoms, indicates the uniform distribution of film surface elements and confirms the incorporation of Sm into the SnO_x matrix.

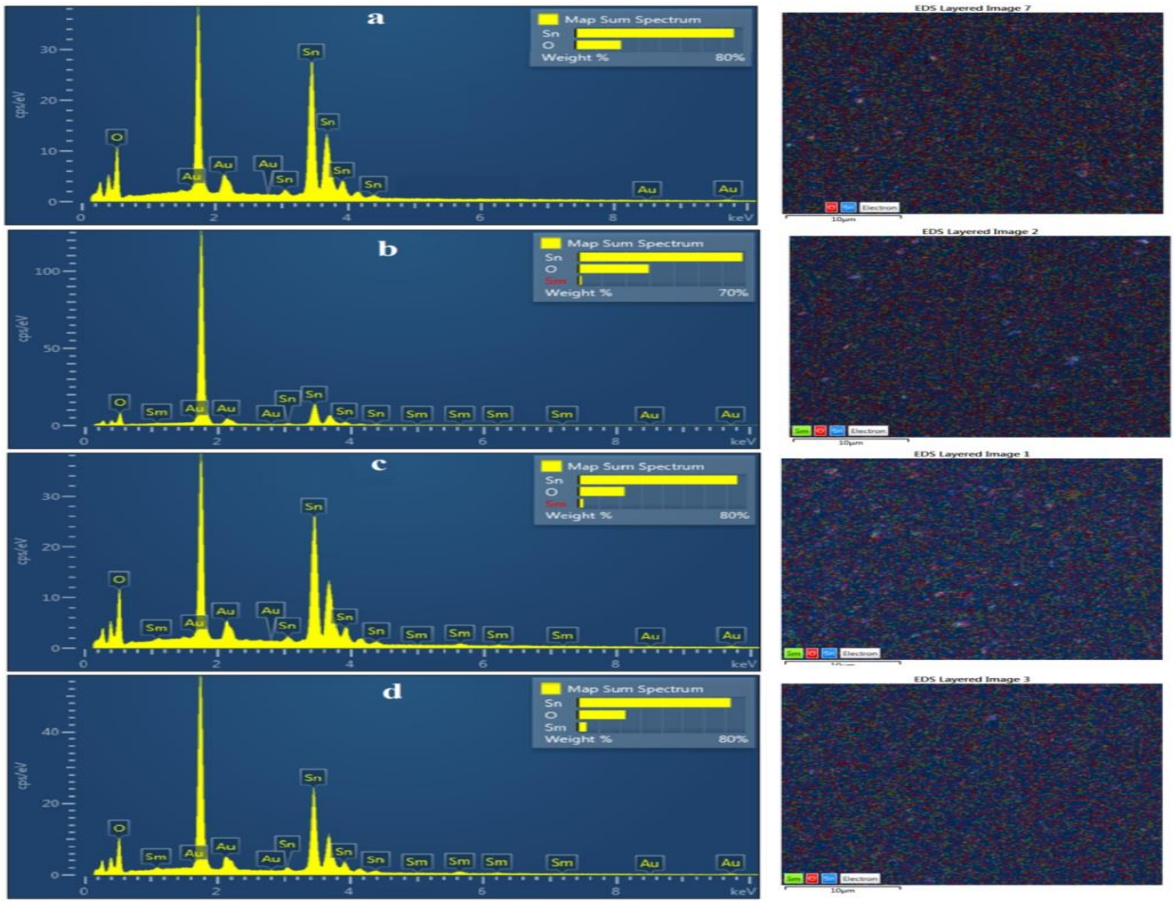

Fig. 6. EDX analysis of (a) the as-deposited SnO_x, (b) 5 wt.% Sm_2O_3 mixed-SnO_x, (c) 7 wt.% Sm_2O_3 mixed-SnO_x, and (d) 9% Sm_2O_3 mixed-SnO_x

3.4 Optical Properties

The transmittance spectrum analysis findings of the as-deposited and SnO_x-mixed Sm_2O_3 thin films are presented in Fig. 7. The average transmittance of the deposited films was determined within the wavelength ranging from 380 nm to 800 nm. The transmittance was determined to be 80%, 72%, 67%, and 63% for the as-deposited SnO_x thin films mixed with 5 wt.%, 7 wt.%, and 9 wt.% Sm_2O_3, respectively. The reduction in transmittance may be ascribed to incorporating samarium into the tin oxide crystals. The samarium atom contributes an extra electron, increasing the concentration of free electrons, enhancing the photon absorption of free carriers, and reducing the optical transmittance of the tin oxide films. Nion *et al.* observed the same behavior when magnesium oxide films were doped with aluminum. [43].

Fig. 7 additionally illustrates periodic fluctuations in the recorded transmittance spectrum. The fluctuation periodicity increased with increasing Sm_2O_3 content, indicating an increasing the film thickness [44]. The fluctuations in the transmittance spectrum result from interference effects on smooth surfaces. Smooth film surfaces reduce scattering and random light refraction, improving interference patterns; Sinha and Ramadan *et al.* recorded the same periodic fluctuations in the transmittance spectrum [45,46].

It is also noted that the optical absorption edge shifted towards longer wavelengths (redshift) with increasing samarium content, indicating a decrease in the optical energy gap [47], as shown in the energy gap results. The shift in the optical absorption edge is ascribed to the structural alterations of the synthesized films, where enhanced crystallinity leads to a shifting of the absorption edge towards longer wavelengths, which decreases extended to localized state transitions caused by the band tails formed by the defects (Sm_2O_3 content within the SnO_x lattice) [48].

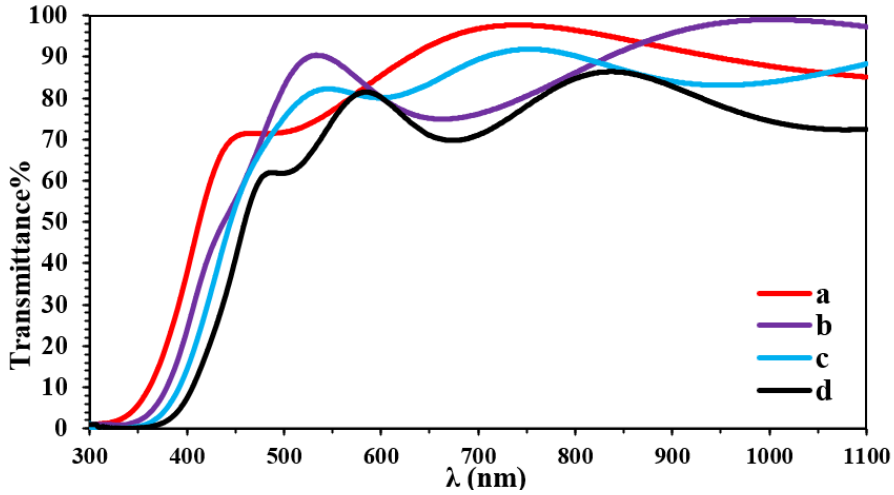

Fig. 7. Optical transmittance spectra of (a) as deposited-SnO_x and SnO_x mixed with (b) 5 wt.% (c) 7 wt.%, and (d) 9 wt.% of Sm_2O_3 thin films

The optical bandgap (Eg^{opt}) was determined using the Tauc relation, Eq (3), as depicted in Fig. 8, which demonstrates that the optical energy gap reduced from 3.4 eV to 3.15 eV with the rise of Sm_2O_3 content in the target to 9 wt.%. Numerous authors have explained the phenomenon of the reduction in the energy gap associated with an increase in particle size, which is further evidenced by a red shift in the absorption edge, as depicted in the optical transmittance spectrum (Fig. 7). This behavior is attributed to bulk defects from incorporating samarium oxide within the tin oxide matrix. These defects have been reported to have reversibly influenced the characteristics of molecular orbitals associated with the conduction band, thereby creating deep electron energy traps and resulting in a reduced energy gap [49–51].

$$\alpha h\upsilon = B(h\upsilon - E_g)^r \tag{3}$$

where $h\upsilon$ is the energy of the absorbed photon, B is a material-dependent constant and r is the exponential coefficient that varies with the type of transitions.

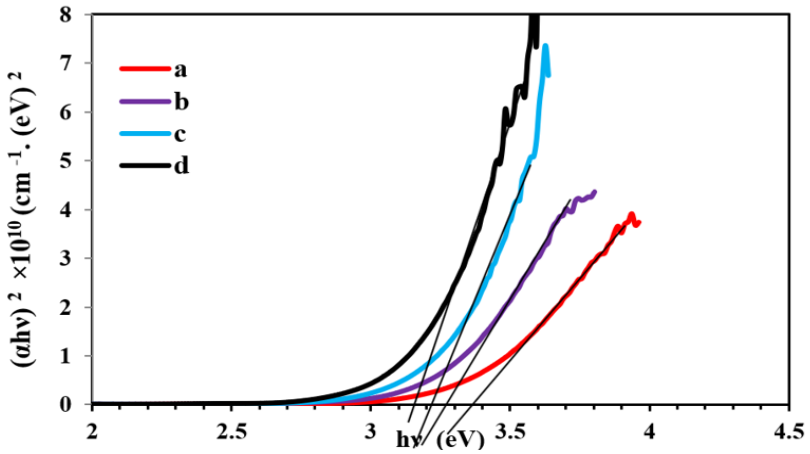

Fig. 8. Tauc-Plot of (a) as deposited-SnO_x and Sm_2O_3-mixed SnO_x at (b) 5 wt.% (c) 7 wt.%, and (d) 9 wt.%

Fig. 9 highlights the investigation's findings regarding average optical transmittance, optical energy gap, and the thickness of the developed films as a function of samarium oxide contents. The maximum content of samarium oxide (9 wt.%) reduced the optical transmittance of the as-deposited tin oxide films by roughly 21%. Reducing optical transmittance can enhance various applications, including protective glasses, solar cells, light filters, optical insulating materials, and light-shielding coatings in surgical and industrial settings. Compared to tin oxide films, samarium oxide contents reduce the energy gap, allowing the deposited films to be used as optical windows in solar cell applications, which allows a wider spectrum of light transmission. Additionally, compared to the as-deposited tin oxide, manufactured coatings can improve the sensitivity and efficiency of optical detectors by enhancing light transmission over a wider wavelength range. The developed films may also increase surface activity and chemical interaction, improving sensor responses against gases [41,52].

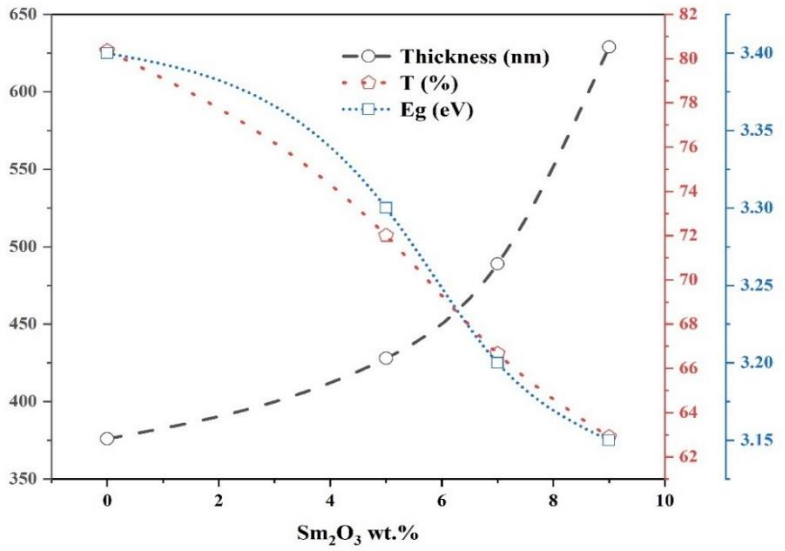

Fig. 9. Variation of optical transmittance, optical energy gap, and the thickness of the developed films as a function of samarium oxide contents

3.4 Photoluminescence results

Fig. 10 presents the photoluminescence spectra of the SnO_x and Sm_2O_3-mixed SnO_x at various wt.% thin films at room temperature, covering the wavelength range of 320 to 560 nm and utilizing an excitation wavelength of λ_{exc}=290 nm. A broad peak was observed in all samples at approximately 361 nm (3.43 eV), attributed to band-to-band transitions [53]. Incorporating the Sm_2O_3 to 9 wt.% caused a red shift in the emission peak up to 387 nm, indicating a reduction in the energy bandgap to 3.2 eV, as listed in Table 4.

Table 4. λ_{max}, Intensity, and corresponding PL emission of SnO_x and SnO_x mixed with Sm_2O_3 at various wt.% concentrations

Sample	λmax (nm)	Intensity (a.u)	Energy (eV)
SnOx	361	10.65	3.43
5 wt.% Sm_2O_3	371	9.55	3.34
7 wt. % Sm_2O_3	382	8.15	3.25
9 wt. % Sm_2O_3	387	6.84	3.2

The energy bandgap values derived from the photoluminescence spectra closely align with those determined using the Tauc relation, showing a decrease from 3.4 eV to 3.15 eV with increasing Sm_2O_3 content. The reduction in emission peak intensity suggests an increase in lattice defects with increasing Sm_2O_3 wt.% [54].

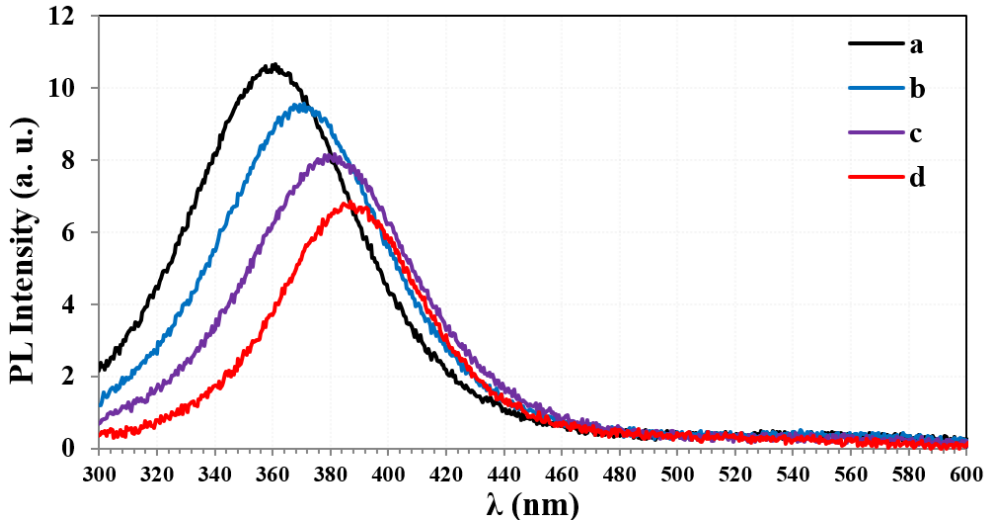

Fig. 10. PL of (a) as-deposited SnOx and Sm_2O_3-mixed SnO_x at (b) 5 wt.% (c) 7 wt.%, and (d) 9 wt.% thin films.

4. Conclusions

In this work, the pulsed laser deposition technique was successfully used to analyze the structural, morphological, and optical characteristics of SnO_x thin films mixed with various weight ratios of samarium oxide. The study demonstrates that Sm_2O_3 mixing significantly influences the structural, morphological, and optical properties of SnO_x thin films. Incorporating samarium oxide improved the crystallization of a polycrystalline structure and reduced the crystal size of tin oxide films. Polycrystalline phases greatly impact electronic applications by improving materials' electrical and thermal performance and supporting the creation of innovative materials with enhanced properties, such as gas sensors and photodetector features.

The morphological analysis revealed an extensive tin oxide thin film surface coated with almost spherical nanoparticles that are randomly distributed, exhibiting a uniform particle size distribution. Adding samarium oxide controls the surface area to volume ratio by reducing the diameters of tin oxide thin film particles, forming a more homogeneous microstructure that improves mechanical properties studies and gas sensor redox reactions. The thickness of the SnO_x thin films increased from 376 nm to 629 nm with the increasing samarium oxide mixing ratio, attributable to the incorporation of Samarium into the SnO_x lattice. This expands the interatomic distance of the SnO_x crystal lattice, enhances lattice parameters, and eventually results in a thicker deposition layer. The maximum content of samarium oxide (9 wt.%) reduced the optical transmittance of the as-deposited tin oxide films by roughly 21%. Reducing optical transmittance can enhance various applications, including protective glasses, solar cells, light filters, optical insulating materials, and light-shielding coatings in surgical and industrial settings. Moreover, reduced energy gap coatings transmit more light across a wider wavelength range for solar cell optical windows, boosting optical detector sensitivity and efficiency. These tunable properties make samarium oxide-mixed SnO_x thin films promising candidates for optoelectronic applications requiring specific optical and surface characteristics.

References

[1] S. P, J. RM, K. DAK, P.S. SK, S. P, L. A. Physical Properties of Rare Earth Metal (Gd3+) Doped SnO2 Thin Films Prepared by Simplified Spray Pyrolysis Technique Using Nebulizer. Optik, 2019; 194: 162887. https://doi.org/10.1016/j.ijleo.2019.05.093

[2] Rzaij JM, Abbas QA, Khalaf AM. Investigating the Structural, Topographical, Morphological and Optical Effects of AgO on Sprayed SnO2 Thin Films. Bulletin of Materials Science, 2023; 46(4): 200. https://doi.org/10.1007/s12034-023-03040-z

[3] Orhan Z, Daş E, Bozkurt G. Microemulsion Synthesis of SnO2 Nanoparticles and Their Integration in Au/n-Si/Al Device Structure. Journal of Materials Science: Materials in Electronics, 2025; 36(2): 158. https://doi.org/10.1007/s10854-025-14242-y

[4] Villamagua L, Stashans A, Lee P, Liu Y, Liu C, Carini M. Change in the Electrical Conductivity of SnO 2 Crystal from n -Type to p -Type Conductivity. CHEMICAL PHYSICS, 2015; 452: 71-77. https://doi.org/10.1016/j.chemphys.2015.03.002
[5] Akkera HS, Kumar Y, Kumar MD, Reddy GS, Kumar BR, Pasha UM, Bitla Y, Ganesh V. Structural, Electrical, and Optical Properties of Rare-Earth Sm3+ Doped SnO2 Transparent Conducting Oxide Thin Films for Optoelectronic Device Applications: Synthesized by the Spin Coating Method. Optical Materials, 2022; 133: 112993. https://doi.org/10.1016/j.optmat.2022.112993
[6] Morais EA de, Scalvi LVA, Cavalheiro AA, Tabata A, Oliveira JBB. Rare Earth Centers Properties and Electron Trapping in SnO2 Thin Films Produced by Sol-Gel Route. Journal of Non-Crystalline Solids, 2008; 354(42-44): 4840-4845. https://doi.org/10.1016/j.jnoncrysol.2008.04.029
[7] Suhail MH. Preparation and Characterization of Mixed SnO2:CdO Thin Films as Gas Sensor. Iraqi Journal of Physics, 2019; 15(33): 28-39. https://doi.org/10.30723/ijp.v15i33.137
[8] Sao AK, Sharma A, Verma M, Tomar M, Chowdhuri A. Development of CdS-SnO2 Hybrid Nanocomposite Thin Films for Trace Level Detection of NO2 Gas. Sensors and Actuators B: Chemical, 2023; 393: 134198. https://doi.org/10.1016/j.snb.2023.134198
[9] Al-Jumaili HS, Jasim MN. Preparation and Characterization of ZnO: SnO2 Nanocomposite Thin Films on Porous Silicon as H2S Gas Sensor. Journal of Ovonic Research, 2019; 15(1): 81-87.
[10] Abuelwafa AA, El-sadek MSA, Elnobi S, Soga T. Effect of Transparent Conducting Substrates on the Structure and Optical Properties of Tin (II) Oxide (SnO) Thin Films: Comparative Study. Ceramics International, 2021; 47(10): 13510-13518. https://doi.org/10.1016/j.ceramint.2021.01.209
[11] Kadhim MA, Ramadhan AA, Al-Gburi MOS. Effect of PEG Addition on an SnO2 Gas Sensor Fabricated Using Spin Coating. Karbala International Journal of Modern Science, 2021; 7(1). https://doi.org/10.33640/2405-609X.2486
[12] Meng D, Liu D, Wang G, Shen Y, San X, Li M, Meng F. Low-Temperature Formaldehyde Gas Sensors Based on NiO-SnO2 Heterojunction Microflowers Assembled by Thin Porous Nanosheets. Sensors and Actuators B: Chemical, 2018; 273: 418-428. https://doi.org/10.1016/j.snb.2018.06.030
[13] Nwanna EC, Imoisili PE, Jen T-C. Synthesis and Characterization of SnO2 Thin Films Using Metalorganic Precursors. Journal of King Saud University - Science, 2022; 34(5): 102123. https://doi.org/10.1016/j.jksus.2022.102123
[14] Ahmadnia-Feyzabad S, Mortazavi Y, Khodadadi AA, Hemmati S. Sm2O3 Doped-SnO2 Nanoparticles, Very Selective and Sensitive to Volatile Organic Compounds. Sensors and Actuators B: Chemical, 2013; 181: 910-918. https://doi.org/10.1016/j.snb.2013.02.101
[15] Singkammo S, Wisitsoraat A, Tuantranont A, Phanichphant S, Yodsri V, Liewhiran C. Catalytic Roles of Sm2O3 Dopants on Ethylene Oxide Sensing Mechanisms of Flame-Made SnO2 Nanoparticles. Applied Surface Science, 2018; 454: 30-45. https://doi.org/10.1016/j.apsusc.2018.05.146
[16] Enad AM, Rzaij JM. Investigate the Structural , Morphological , and Topographical Characteristics of CuO Thin Films Utilizing a Pulsed Laser Deposition Method. Journal of Theoretical and Applied Physics, 2024; 18(AICIS'23): 1-8.
[17] Conde Garrido JM, Silveyra JM. A Review of Typical PLD Arrangements: Challenges, Awareness, and Solutions. Optics and Lasers in Engineering, 2023; 168: 107677. https://doi.org/10.1016/j.optlaseng.2023.107677
[18] Devitsky O V., Kravtsov AA. Effect of Thermal Annealing on the Structural Evolution of Thin Ceramic YAG: Ce Films Grown by Pulsed Laser Deposition. Ceramics International, 2024. https://doi.org/10.1016/j.ceramint.2024.12.047
[19] Pashchenko AS, Devitsky O V., Lunina ML, Danilina EM, Pashchenko OS, Ber B, Sakharov VI. Epitaxial Growth of GaInAsBi Thin Films on Si (001) Substrate Using Pulsed Laser Deposition. Vacuum, 2024; 227: 113372. https://doi.org/10.1016/j.vacuum.2024.113372
[20] Lorenz M, Hochmuth H, von Wenckstern H, Grundmann M. Flexible Hardware Concept of Pulsed Laser Deposition for Large Areas and Combinatorial Composition Spreads. Review of Scientific Instruments, 2023; 94(8). https://doi.org/10.1063/5.0142085
[21] Xu H, Li J, Li P, Shi J, Gao X. Effect of Rare Earth Doping on Electronic and Gas-Sensing Properties of SnO2 Nanostructures. Journal of Alloys and Compounds, 2022; 909: 164687. https://doi.org/10.1016/j.jallcom.2022.164687
[22] Mohammed Enad A, Rzaij JM. Synthesis of CuO Thin Film Incorporated with Nanostructured Nd 2 O 3 Deposited by Pulsed Laser Deposition for Ammonia Sensing Applications. Nano, 2024. https://doi.org/10.1142/S1793292024501133
[23] Madkhali O. A Review of Novel Methods to Improve the Optical and Electrical Properties of N-Type and p-Type Sulphides and Oxides: Leading the Frontiers of Semiconductor Technology. Physica Scripta, 2024; 99: 022004. https://doi.org/10.1088/1402-4896/ad1e44

[24] Tepamatr P, Laosiripojana N, Sesuk T, Charojrochkul S. Effect of Samarium and Praseodymium Addition on Water Gas Shift Performance of Co/CeO2 Catalysts. Journal of Rare Earths, 2020; 38(11): 1201-1206. https://doi.org/10.1016/j.jre.2019.12.003
[25] Kumar A, Kumar N, Chitkara M, Dhillon G. Physicochemical Investigations of Structurally Enriched Sm3+ Substituted SnO2 Nanocrystals. Journal of Materials Science: Materials in Electronics, 2022; 33(8): 5283-5296. https://doi.org/10.1007/s10854-022-07716-w
[26] Xu Y, Yang L, Li J, Zhou D, Li Q, Shi W, Jin Y. Effect of Laser Wavelength on Ablation Propulsion and Plasma Characteristics with Acrylonitrile Butadiene Styrene Target. Journal of Physics D: Applied Physics, 2024; 57(44): 445201. https://doi.org/10.1088/1361-6463/ad6877
[27] Nikiforov A, Timofeev V, Mashanov V, Azarov I, Loshkarev I, Volodin V, Gulyaev D, Chetyrin I, Korolkov I. Formation of SnO and SnO2 Phases during the Annealing of SnO(x) Films Obtained by Molecular Beam Epitaxy. Applied Surface Science, 2020; 512: 145735. https://doi.org/10.1016/j.apsusc.2020.145735
[28] Ding X, Fang F, Jiang J. Electrical and Optical Properties of N-Doped SnO 2 Thin Films Prepared by Magnetron Sputtering. Surface and Coatings Technology, 2013; 231: 67-70. https://doi.org/10.1016/j.surfcoat.2012.03.060
[29] Ebrahimiasl S, Yunus WMZW, Kassim A, Zainal Z. Synthesis of Nanocrystalline SnOx (x = 1-2) Thin Film Using a Chemical Bath Deposition Method with Improved Deposition Time, Temperature and PH. Sensors, 2011; 11(10): 9207-9216. https://doi.org/10.3390/s111009207
[30] Singh LP, Luwang MN, Srivastava SK. Luminescence and Photocatalytic Studies of Sm 3+ Ion Doped SnO 2 Nanoparticles. New J. Chem., 2014; 38(1): 115-121. https://doi.org/10.1039/C3NJ00759F
[31] Anthopoulos TD, Mclachlan MA. Exploring and Controlling Intrinsic Defect Formation in SnO2 Thin Films. Journal of Materials Chemistry C, 2016; 4: 758-765. https://doi.org/10.1039/C5TC03520A
[32] Cao E, Zhang Y, Hao W, Peng H, Sun L, Hu J. Applied Surface Science Room Temperature Ferromagnetism in Sm-Doped SnO 2 PLD Film. Applied Surface Science, 2013; 282: 376-383. https://doi.org/10.1016/j.apsusc.2013.05.139
[33] E. WB. X-Ray Diffraction. New York: Dover Publications 1990;
[34] Heryanto, Abdullah B, Tahir D, Mahdalia. Quantitative Analysis of X-Ray Diffraction Spectra for Determine Structural Properties and Deformation Energy of Al, Cu and Si. Journal of Physics: Conference Series, 2019; 1317(1): 012052. https://doi.org/10.1088/1742-6596/1317/1/012052
[35] Shawki OS, Rzaij JM. Effect of Fe2O3 Upper Layer on Structural, Morphological, and Photoluminescence Characteristics of TiO2 Thin Film Prepared by Chemical Spray Pyrolysis. In:. 1st Diyala Int. Conf. Pure Appl. Sci. Iraq: AIP Conference Proceedings 2023; 020009. https://doi.org/10.1063/5.0112172
[36] T.O. O, K.O. A, S.O. O. Estimation Of The Atomic Radii Of Periodic Elements Using Support Vector Machine. International Journal of Advanced Information Science and Technology, 2014; 28(28): 39-49. https://doi.org/10.15693/IJAISTAUG001/001
[37] Sen P, Bhattacharya P, Mukherjee G, Ganguly J, Marik B, Thapliyal D, Verma S, Verros GD, Chauhan MS, Arya RK. Advancements in Doping Strategies for Enhanced Photocatalysts and Adsorbents in Environmental Remediation. Technologies, 2023; 11(5): 144. https://doi.org/10.3390/technologies11050144
[38] Baig N, Kammakakam I, Falath W. Nanomaterials: A Review of Synthesis Methods, Properties, Recent Progress, and Challenges. Materials Advances, 2021; 2(6): 1821-1871. https://doi.org/10.1039/D0MA00807A
[39] Modhi MK, Rzaij JM. Synthesis and Characterization Study of CuO Thin Film and CuO-CeO2 Nanostructured Composite Using Chemical Spray Pyrolysis. In:. AL-KADHUM 2ND Int. Conf. Mod. Appl. Inf. Commun. Technol. Baghdad, Iraq: AIP Conference Proceedings 2023; 030066. https://doi.org/10.1063/5.0120468
[40] Li L, Zhou C, Yu D, Zheng Y, Du Y, Ma L, Zhao J, Rao G. Effect of Film Thickness on the Microstructure and Dielectric and Ferroelectric Properties of (Bi0.5Na0.5)0.94Ba0.06TiO3 Films by Pulsed Laser Deposition. Journal of Electronic Materials, 2023; 52(5): 3488-3498. https://doi.org/10.1007/s11664-023-10321-0
[41] Ibraheam AS, Rzaij JM, Arshad MKM. Influence of Magnesium Content on the Structural, Optical, and Electrical Properties of Cu2(Zn1-XMgx)SnS4 Nanostructured Quaternary Thin Film Synthesized Using the Sol-Gel Method. Journal of Electronic Materials, 2023; 52(1): 414-421. https://doi.org/10.1007/s11664-022-10002-4
[42] Nix WD. Mechanical Properties of Thin Films. Metallurgical Transactions A, 1989; 20(11): 2217-2245. https://doi.org/10.1007/BF02666659
[43] Golam Mortuza Nion M, Humayan Kabir M, Mona MA, Jahidul Haque M, Shahariar N, Hafiz M, Rahman MS. Effect of Al Doping on Morphology and Optical Properties of Spray Pyrolized MgO Thin Films. Results in Materials, 2021; 12: 100235. https://doi.org/10.1016/j.rinma.2021.100235
[44] Chowdhury FR, Choudhury S, Hasan F, Begum T. Optical Properties of Undoped and Indium-Doped Tin Oxide Thin Films. Journal of Bangladesh Academy of Sciences, 2011; 35(1): 99-111. https://doi.org/10.3329/jbas.v35i1.7975

[45] Ramadan R, Abdelhady K, Manso-Silván M, Torres-Costa V, Martín-Palma RJ. Microwave Plasma and Rapid Thermal Processing of Indium-Tin Oxide Thin Films for Enhancing Their Performance as Transparent Electrodes. Journal of Photonics for Energy, 2019; 9(03): 1. https://doi.org/10.1117/1.JPE.9.034001
[46] K. Sinha S. Tunable Structural, Optical And Electrical Properties Of Annealed ZnO-SnO2 Composite Thin Films Deposited By Pulsed Laser Deposition. Advanced Materials Letters, 2016; 7(4): 319-324. https://doi.org/10.5185/amlett.2016.6155
[47] Tawfeeq HA, Rzaij JM. Effect of Thickness on the Structural and Optical Properties of Cadmium Oxide Thin Films Deposited by Thermal Vacuum Evaporation Technique. In:. Recent Trends Adv. Artif. Intell. Internet Things. Springer International Publishing 2024; 582-591. https://doi.org/10.1007/978-3-031-70924-1_44
[48] Buchholz DB, Proffit DE, Wisser MD, Mason TO, Chang RPH. Electrical and Band-Gap Properties of Amorphous Zinc-Indium-Tin Oxide Thin Films. Progress in Natural Science: Materials International, 2012; 22(1): 1-6. https://doi.org/10.1016/j.pnsc.2011.12.001
[49] ŞİMŞEK T, CEYLAN A, AŞKIN GŞ, ÖZCAN Ş. Band Gap Engineering of ZnO Nanocrystallites Prepared via Ball-Milling. Politeknik Dergisi, 2022; 25(1): 89-94. https://doi.org/10.2339/politeknik.647702
[50] LIN H, HUANG C, LI W, NI C, SHAH S, TSENG Y. Size Dependency of Nanocrystalline TiO2 on Its Optical Property and Photocatalytic Reactivity Exemplified by 2-Chlorophenol. Applied Catalysis B: Environmental, 2006; 68(1-2): 1-11. https://doi.org/10.1016/j.apcatb.2006.07.018
[51] Brus L. Electronic Wave Functions in Semiconductor Clusters: Experiment and Theory. The Journal of Physical Chemistry, 1986; 90(12): 2555-2560. https://doi.org/10.1021/j100403a003
[52] Tawfeeq HA, Rzaij JM. The Effect of Nb2O5 and Pdo Nanostructures Coating on the Structural and Morphological Properties of CdO Thin Films. In:. 4TH Int. Conf. PURE Sci. ICPS2023. Baghdad, Iraq: 2024; 050011. https://doi.org/10.1063/5.0196260
[53] Li N, Fan Y, Shi Y, Xiang Q, Wang X, Xu J. A Low Temperature Formaldehyde Gas Sensor Based on Hierarchical SnO/SnO2 Nano-Flowers Assembled from Ultrathin Nanosheets: Synthesis, Sensing Performance and Mechanism. Sensors and Actuators, B: Chemical, 2019; 294(January): 106-115. https://doi.org/10.1016/j.snb.2019.04.061
[54] Rzaij JM. A Novel Room-Temperature Nitrogen Dioxide Gas Sensor Based on Silver-Doped Cerium Oxide Thin Film. Sensors and Actuators A: Physical, 2023; 363: 114748. https://doi.org/10.1016/j.sna.2023.114748